Chromophore Orientation in Bacteriorhodopsin Determined from the Angular Dependence of Deuterium Nuclear Magnetic Resonance Spectra of Oriented Purple Membranes†

Stephan Moltke,‡ Alexander A. Nevzorov,‡ Naomi Sakai,§ Ingrid Wallat,|| Constantin Job,⊥ Koji Nakanishi,§ Maarten P. Heyn,*,|| and Michael F. Brown‡

Department of Chemistry, University of Arizona, Tucson, Arizona 85721, Department of Chemistry, Columbia University, New York, New York 10027, Department of Physics, Freie Universität Berlin, Arnimallee 14, D-14195 Berlin, Germany, and Arizona Research Laboratories, University of Arizona, Tucson, Arizona 85721

Received March 24, 1998

ABSTRACT: The orientation of prosthetic groups in membrane proteins is of considerable importance in understanding their functional role in energy conversion, signal transduction, and ion transport. In this work, the orientation of the retinylidene chromophore of bacteriorhodopsin (bR) was investigated using ^{2}H NMR spectroscopy. Bacteriorhodopsin was regenerated with all-trans-retinal stereospecifically deuterated in one of the geminal methyl groups on C_1 of the cyclohexene ring. A highly oriented sample, which is needed to obtain individual bond orientations from ^{2}H NMR, was prepared by forming hydrated lamellar films of purple membranes on glass slides. A Monte Carlo method was developed to accurately simulate the ^{2}H NMR line shape due to the distribution of bond angles and the orientational disorder of the membranes. The number of free parameters in the line shape simulation was reduced by independent measurements of the intrinsic line width (1.6 kHz from T_{2e} experiments) and the effective quadrupolar coupling constant (38.8−39.8 kHz from analysis of the line shape of a powder-type sample). The angle between the C_1−(1*R*)-1-CD_3 bond and the purple membrane normal was determined with high accuracy from the simultaneous analysis of a series of ^{2}H NMR spectra recorded at different inclinations of the uniaxially oriented sample in the magnetic field at 20 and −50 °C. The value of 68.7 ± 2.0° in dark-adapted bR was used, together with the previously determined angle of the C_5−CD_3 bond, to calculate the possible orientations of the cyclohexene ring in the membrane. The solutions obtained from ^{2}H NMR were then combined with additional constraints from linear dichroism and electron cryomicroscopy to obtain the allowed orientations of retinal in the noncentrosymmetric membrane structure. The combined data indicate that the methyl groups on the polyene chain point toward the cytoplasmic side of the membrane and the N−H bond of the Schiff base to the extracellular side, i.e., toward the side of proton release in the pump pathway.

The integral membrane protein bacteriorhodopsin (bR)[1] found in the purple membrane of the archaebacterium *Halobacterium salinarium* belongs to the important family of seven transmembrane helix proteins and is a model system for active proton transport. The retinal chromophore of this light-driven proton pump and its Schiff base linkage to the protein clearly play a central role in the molecular mechanism of proton transport. Not only is the chromophore involved in the primary step of light absorption and the subsequent isomerization steps, but its protonated Schiff base linkage is also the source of the transported proton. Therefore, knowledge of the chromophore conformation and orientation within the membrane and its changes during the photocycle is of great interest, and an important element in understanding the transport mechanism. The position of the chromophore both within the plane of the membrane and perpendicular to it has been determined by neutron diffraction using purple membranes regenerated with specifically deuterated retinals (*1*, *2*). The chromophore has also been modeled into the electron density map obtained from electron cryomicroscopy (*3*) using the X-ray structure of a retinal model compound (*4*). This map has a resolution of 3.5 and 4.3 Å in the directions parallel and perpendicular to the plane of the membrane, respectively. Most recently, this structure has also been used as a starting point for the refinement of the electron density map determined from X-ray diffraction of microcrystals (*5*). In all of these cases, initial assumptions about the orientation of the retinal chromophore within the membrane frame are necessary, and the structure and orientation of the retinal chromophore are not yet known with certainty.

† Work supported by grants from the National Institutes of Health (GM 53484 to M.P.H., EY 10622 and EY 12049 to M.F.B., and GM 36564 to K.N.) and a postdoctoral fellowship from the Deutsche Forschungsgemeinschaft (to S.M.).

* To whom correspondence should be addressed.
‡ Department of Chemistry, University of Arizona.
§ Columbia University.
|| Freie Universität Berlin.
⊥ Arizona Research Laboratories, University of Arizona.

[1] Abbreviations: bR, bacteriorhodopsin; D, deuterium; Dibal, diisobutylaluminum hydride; FTIR, Fourier transform infrared spectroscopy; HOOP, hydrogen-out-of-plane mode; NMR, nuclear magnetic resonance spectroscopy; ^{2}H NMR, deuterium nuclear magnetic resonance; TLC, thin-layer chromatography.

S0006-2960(98)00676-X CCC: $15.00
Published on Web 08/05/1998

The local structure of integral membrane proteins can be investigated using diffraction methods with isomorphic labels (*1*, *2*, *6*) or solid-state NMR (*7*), including magic angle spinning (*8*, *9*), rotational resonance (*10*, *11*), and rotational echo double resonance (REDOR) (*12*−*15*). With the latter NMR methods, randomly oriented samples are used and one obtains internuclear distances, i.e., distance constraints. However, orientational information from tensorial interactions, e.g., the orientation of the principal axis system with respect to the membrane frame, is unavailable in these experiments. An alternative strategy involves solid-state NMR of oriented systems, which provides orientational constraints on individual bond angles with respect to the axis of orientation. The information about bond angles is complementary to the distance information. For instance, solid-state wide-line ^{2}H NMR spectroscopy of oriented samples can be used to directly measure the orientation of ^{2}H-labeled bonds relative to the membrane frame with high accuracy (*16*, *17*). Such an approach has been employed successfully for gramicidin A to determine a high-resolution structure from the orientational constraints on single bond directions (*18*, *19*). For bacteriorhodopsin, encouraging results have been obtained previously for selected bonds of the chromophore in the dark-adapted ground state (*20*, *21*) and in the M intermediate (*22*). The angles between the C−CD_3 bond and the membrane normal have been reported for the methyl groups on C_5, C_9, and C_{13} (for the numbering scheme, cf. Figure 1a). It was concluded that the polyene chain of the retinal is not straight but curved as observed in crystals of retinal model compounds (*4*).

With regard to understanding the mechanism and vectoriality of proton transport in bR, an important question is the orientation of the retinal within the membrane-embedded protein. In the all-trans form, the retinal has a 6-s-trans conformation (*23*−*27*) and the configuration of the C=N bond of the Schiff base is anti (*28*). Therefore, the methyl groups of the polyene chain on the one hand and the Schiff base N−H bond on the other point to opposite sides of the long axis of the molecule. The same is true for the 13-cis form present in the dark-adapted state of bacteriorhodopsin which has a C=N syn configuration. The cyclohexene ring is closest to the extracellular surface of bR (*29*), with the Schiff base approximately in the middle of the membrane (*2*), and the polyene chain making an angle of about 70 ± 5° with the membrane normal (*30*, *31*). Second-harmonic interference experiments also show that the vector from the cyclohexene ring to the Schiff base points toward the cytoplasmic side of the membrane (*32*). Because the plane of the chromophore is approximately perpendicular to the membrane plane (*33*), this leaves two possible geometries for the overall orientation of the chromophore in the membrane. Either the N−H bond of the Schiff base points toward the cytoplasmic side of the membrane and the methyl groups on C_5, C_9, and C_{13} point toward the extracellular surface (Figure 1b), or the opposite is true (Figure 1c). Several independent experiments using linear dichroism (*31*), neutron diffraction (*2*), and ^{2}H NMR (*20*) suggest that the Schiff base N−H bond points toward the extracellular side. Bioorganic experiments with various retinal analogues, on the other hand, are only consistent with the N−H bond pointing toward the cytoplasmic side (*34*, *35*). Therefore, the orientation of the retinylidene chromophore in bR is an open question at present.

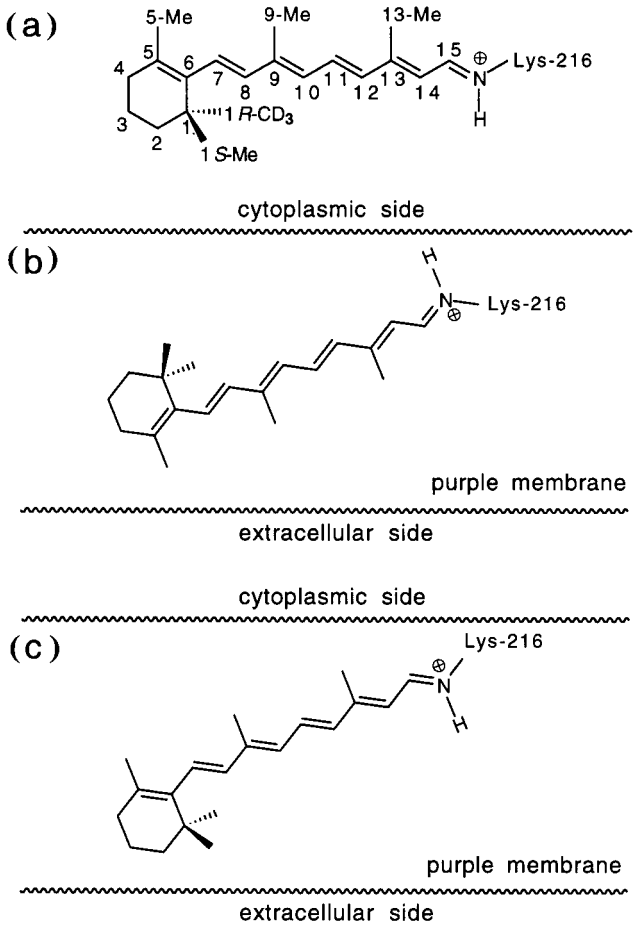

FIGURE 1: (a) Numbering scheme for the retinylidene Schiff base in bR. Me stands for a methyl group, CH_3. In the all-trans form of retinal, the conformation of the Schiff base C=N bond is 15-anti. The C_6−C_7 single bond is 6-s-trans in both the light- and dark-adapted forms of bacteriorhodopsin. (b and c) The retinal chromophore within the purple membrane. The polyene chain makes an angle of 20−25° with the membrane surface, and the cyclohexene ring is known to be located closer to the extracellular side. Therefore, two orientations of the retinal are possible. In panel b, the Schiff base N−H bond points toward the cytoplasmic side, while in panel c, it points toward the extracellular side. The orientation of the methyl groups on the cyclohexene ring with respect to the membrane is also different in the two configurations.

To gain further insight into the chromophore orientation in bR and to discriminate between the above possibilities, we have utilized solid-state ^{2}H NMR to investigate the bond angle with respect to the membrane normal for a stereospecifically labeled methyl group on the ring C_1. An essential requirement of our approach is a high degree of orientational order of the membranes. This was achieved by forming hydrated films of purple membranes on glass plates. For the first time, ^{2}H NMR data were collected with such samples at room temperature (20 °C) and 86% relative humidity. In contrast to electron cryomicroscopy (*29*) and X-ray diffraction (*5*) experiments, which are performed at very low temperatures and with dehydrated samples, our studies were carried out under nearly physiological conditions. An accurate solid-state NMR line shape simulation method was employed which properly accounts for the three-dimensional disorder (mosaic spread) of immobilized uniaxially oriented purple membrane films, using a numerical method that allows a straightforward and exact treatment of the complex

Scheme 1

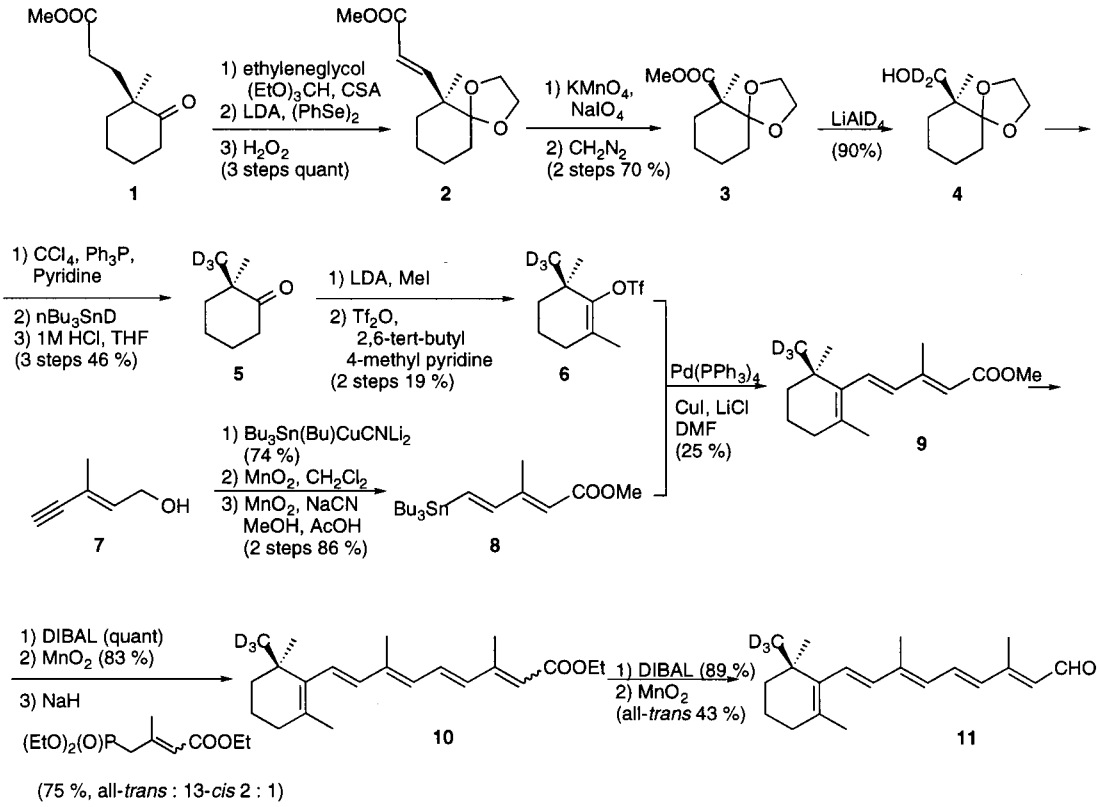

geometry of the sample. From the simulation of the experimental data, we obtain precise information about the orientation of the specifically deuterated bonds with respect to the axis of orientation, i.e., the membrane normal. This knowledge is complementary to the results of other structural methods such as X-ray crystallography (*5*), neutron diffraction (*1*), and electron cryomicroscopy (*3*). The combination of methods which are insensitive to the vectorial orientation of retinal, such as ^{2}H NMR of the methyl groups and linear dichroism (*30*, *31*), together with methods which do depend on its vectorial orientation, such as electron cryomicroscopy (*3*, *29*) and nonlinear optical interference measurements (*32*), yields a more detailed conclusion than any of these experiments alone. By combining the angular constraints from the various techniques, we determined the orientation of the chromophore in the binding pocket of bR. The approach developed in this work may also be applied to other integral membrane proteins containing bound ligands or prosthetic groups implicated in their biological function provided that the group in question can be specifically deuterated and that well-oriented samples can be prepared.

MATERIALS AND METHODS

Stereospecific Deuterium Labeling of Retinal. The synthetic pathway for (1*R*)-[1-CD_3]-all-trans-retinal is summarized in Scheme 1. Commercially available methyl (*S*)-(+)-1-methyl-2-oxocyclohexanepropionate (**1** in Scheme 1, purchased from Aldrich, Milwaukee, WI) was used as the starting material. After protection of the ketone group, a phenyl selenyl group was introduced and subsequently oxidatively removed to yield the unsaturated ester (**2**). The cleavage of the double bond was followed by an esterification to produce the ester (**3**). The ester functional group was converted into a deuterated methyl CD_3 group in three steps. First, the ester was reduced to CD_2OH using $LiAlD_4$, yielding compund **4**. In a second step, the alcohol was converted to the chloride, and third, the chlorine was reductively displaced with deuterium. Deprotection of the ketone group yielded the deuterated 2,2-dimethylcyclohexanone (**5**), which in turn was converted to the cyclohexene ring component (**6**) by α-methylation and enol triflation. The resulting cyclohexene ring (**6**) was coupled with the vinyl tin reagent (**8**) in the presence of a palladium catalyst (*36*) to produce the deuterium-labeled *β*-ionylidene acetate (**9**). Reagent **8** was prepared from trans-3-methyl-2-penten-4-yn-1-ol (**7**, Aldrich) by hydrostannylation (*37*) and oxidation (*38*). The reduction of the resulting ester **9**, oxidation, and a Horner−Emmons reaction gave a mixture of deuterated all-trans- and 13-cis-ethyl retinoate (**10**) in a 2:1 ratio, which was used for the next reaction without further separation. The final reduction with Dibal and oxidation produced the deuterium-labeled retinal as a mixture of double bond isomers. The (1*R*)-[1-CD_3]-all-trans-retinal (**11**) was isolated from the mixture by preparative TLC. The spectral data were consistent with the proposed structure.

(1*R*)-[1-CD_3]-all-trans-Retinal (**11**): ^{1}H NMR (400 MHz, C_6D_6) δ 10.18 (d, 1H, J = 7.8 Hz), 6.98 (dd, 1H, J = 11.5 and 15.2 Hz), 6.53 (d, 1H, J = 16.0 Hz), 6.43 (d, 1H, J = 16.0 Hz), 6.18 (d, 1H, J = 11.5 Hz), 6.18 (d, 1H, J = 15.2 Hz), 6.12 (d, 1H, J = 7.8 Hz), 2.12 (m, 2H), 1.93 (s, 6H), 1.87 (s, 3H), 1.74 (m, 2H), 1.63 (m, 2H), 1.28 (s, 3H); MS (EI) *m*/*z* 287 (M^+); HRMS (EI) *m*/*z* calcd for $C_{20}H_{25}D_3O$ 287.2328, found 287.2336.

Sample Preparation. Purple membranes, containing bR as the only protein component, were isolated from *H. salinarium* strain ET1001 using standard procedures (*39*).

The protein was then bleached by actinic light (>510 nm) in the presence of hydroxylammonium chloride at pH 7, leading to the formation of retinaloxime. The absorption spectrum of this apomembrane suspension had no residual absorbance at 570 nm, showing that the native chromophore was completely removed from the protein. The apomembranes were then regenerated with the (1*R*)-[1-CD_3]-all-trans-retinal in ethanol. They were titrated spectroscopically until excess retinal became observable at 380 nm. Retinaloxime and excess retinal were removed by washing the membranes seven times by centrifugation with bovine serum albumin in MilliQ water. The final product showed no absorption at 380 nm, and the ratio of absorbance at 280 nm to 570 nm was about 1.5, indicating that no albumin remained adsorbed to the membranes. The degree of regeneration as calculated from the absorbance at 570 nm was 92−100%. In the last washing cycle, deuterium-depleted water (Cambridge Isotope Laboratories, Andover, MA; 2−3 ppm ^2H) was used to minimize unwanted contributions from natural abundance HDO in the NMR spectrum. This material was used to prepare both an oriented sample and a powder-type sample. For the oriented sample, a highly concentrated suspension of membranes was applied to a thin glass slide (0.3 mm thickness) on an area about 20 mm long and 5−8 mm wide. The suspension was dried slowly (48 h) in the presence of a saturated solution of KCl in ^2H-depleted water at room temperature to provide a constant relative humidity of about 86%. In this way, highly oriented uniaxial purple membrane films were formed. Neutron diffraction experiments have shown that these films possess a high degree of orientation (low mosaic spread) with the membrane plane parallel to the glass surface (*2*). A total amount of 84 mg of bacteriorhodopsin was applied to 32 plates. Use of spacers at the end of the 30 mm long glass plates allowed sandwiching of two plates with the films facing each other without touching. The 16 sandwiches were fitted into a cutoff Pyrex NMR tube with a 10 mm diameter and a 30 mm length. Removing the plug on the end of the tube allowed rehydration of the sample at 86% relative humidity. The sample tube was sealed for the experiments and used for up to 3 days without rehydrating it. For the powder-type sample, the purple membrane suspension was concentrated by vacuum centrifugation and transferred to a 10 mm × 30 mm NMR tube. The powder-type sample contained 45 mg of bacteriorhodopsin.

Solid-State Deuterium NMR Spectroscopy. NMR experiments were performed using a wide-bore 300 MHz magnet (7.05 T) and a Bruker (Billerica, MA) AMX console. Probeheads with a horizontal solenoidal coil having a 10 mm diameter and a 20 mm length were home-built. The deuterium resonance at 46.13 MHz was determined by using D_2O with a line width of 5 Hz. The acquisition parameters for the quadrupolar echo sequence ($90°_x$−delay−$90°_y$−delay−acquire) were determined from a perdeuterated plexiglass powder sample. Using a 1 kW Henry radio amplifier (Henry Radio, Los Angeles, CA), the 90° pulse length was 3.2 μs. The pulse delays and reference phase were chosen such that no distortion or asymmetry of the plexiglass line shape was detectable in a comparison with the simulated powder-type line shape, for both the CD_3 and CD_2 signals. Thus, a pulse delay of 45 μs was sufficient to avoid artifacts due to probe ringing. The recycle time was chosen to be 200 ms, in accordance with the experimentally determined values of the spin−lattice relaxation time T_{1Z} of 74 ± 7 ms at 20 °C and 23 ± 4 ms at −50 °C (from inversion recovery experiments with the oriented bR sample, data not shown). The dwell time of the experiments was set to 0.5 μs with 4096 points acquired at 12 bit resolution. A standard eight-step phase cycle was employed to eliminate artifacts arising from differences in the two quadrature detection channels (*40*). Under these conditions, a powder pattern from natural abundance deuterium in hexamethylbenzene can be recorded in 250 000 acquisitions with a signal-to-noise ratio of 30. The spectral width of the 3.2 μs pulses is large enough to detect a powder pattern from methylene deuterons, whose quadrupolar coupling constant is about 3 times that of deuterons in a rapidly rotating methyl group. In general, a 2 kHz exponential multiplication was applied to the quadrupolar echo to increase the signal-to-noise ratio. For the experiments with the oriented films of purple membranes, the orientation of the sample relative to the magnetic field is an important parameter (see below). The sample tilt is the angle between the normal to the glass plates and the magnetic field. This angle was set manually in steps of 15 ± 3° by rotating the sample tube in the horizontal coil. Thus, spectra at seven different tilt angles from 0 to 90° were recorded under otherwise identical conditions.

Simulation of Deuterium NMR Line Shapes. The quadrupolar interaction between the electric field gradient at the deuterium nucleus and its electric quadrupolar moment is an orientation-dependent perturbation which shifts the Zeeman levels of the nucleus. Therefore, the two transitions of the deuterium nucleus have different energies, and one observes two lines symmetric about the Larmor frequency, whose splitting is given in a first-order approximation by (*16*, 17)

$$\Delta\nu_Q = \frac{3}{2}\chi_Q^{\mathrm{stat}}\left\{D_{00}^{(2)}(\Omega_{PL}) - \frac{\eta_Q^{\mathrm{stat}}}{\sqrt{6}}[D_{-20}^{(2)}(\Omega_{PL}) + D_{20}^{(2)}(\Omega_{PL})]\right\} \quad (1)$$

where χ_Q^{stat} (≃170 kHz) is the static quadrupolar coupling constant for a C−D bond (*16*), $D_{m0}^{(2)}(\Omega_{PL})$ are Wigner rotation matrix elements of rank 2, $\Omega_{PL} = (\alpha_{PL},\beta_{PL},0)$ are the Euler angles for the transformation from the principal axis system of the field gradient to the laboratory system of the magnetic field, and $\eta_Q^{\mathrm{stat}} = (V_{yy} - V_{xx})/V_{zz}$ is the asymmetry parameter of the electric field gradient tensor. For a deuterated methyl group, the fast rotation around the C−C axis preaverages the interaction, and χ_Q^{stat} and η_Q^{stat} have to be replaced by an effective coupling constant χ_Q^{eff} and an effective asymmetry parameter η_Q^{eff}, respectively. For the methyl rotor, χ_Q^{eff} has a value of approximately $-{}^1/_3\chi_Q^{\mathrm{stat}}$, and the effective asymmetry parameter is sufficiently small that it can be set to zero without loss of precision. Therefore, the above expression can be simplified to

$$\Delta\nu_Q = \Delta\nu_Q^{\mathrm{powder}}(3\cos^2\theta - 1) \quad (2)$$

The angle θ is the angle between the C−C bond and the magnetic field. With only one orientation present in the sample, the spectrum would consist of just two lines, while

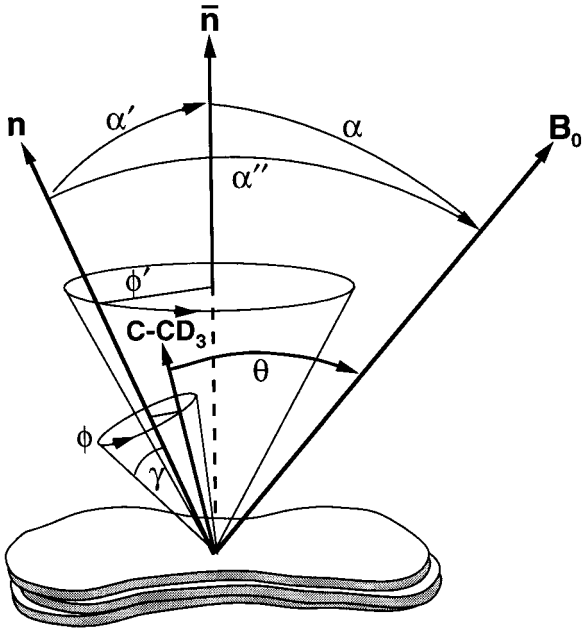

FIGURE 2: Geometry of a uniaxially oriented sample. For a deuterated methyl group, the quadrupolar frequency shift depends on the angle θ between the C−CD_3 bond and the magnetic field $\mathbf{B_0}$. To describe the disorder in the sample, two intermediate frames of reference are introduced. In the local membrane frame, the angle the C−CD_3 bond makes with the local membrane normal **n** is called γ. Since the purple membranes are randomly oriented in-plane, the bond vectors lie on a cone with angle γ and it is assumed that all azimuthal angles ϕ are equally probable. The individual normals **n** are not perfectly aligned, but are assumed to be distributed in a Gaussian manner in space. The two angles α' and ϕ' describe this distribution, where α' is normally distributed about the average membrane normal $\bar{\mathbf{n}}$ with an additional weighting factor sin α' to account for the volume element in spherical polar coordinates, and the azimuth ϕ' is again uniformly distributed. The inclination of the sample, i.e., the angle between the average normal $\bar{\mathbf{n}}$ and the magnetic field $\mathbf{B_0}$, is called α.

the line shape is more complex if more than one orientation is present. In this case, the line shape reflects the orientational probability distribution of the bond angles (*16*, *17*). For an isotropic distribution (powder-type sample), the result is the well-known Pake pattern. Here, the constant $\Delta\nu_Q^{\text{powder}}$ ($=^3/_4\chi_Q^{\text{eff}}$) can be directly determined as the frequency separation of the two prominent horns or edges corresponding to a 90° orientation, for which the factor (3 cos^2 θ − 1) equals −1. However, even for a perfectly oriented sample, eq 2 still is not unambiguous. First, angles θ and $\pi - \theta$ result in the same splitting. Second, since only the absolute value of $\Delta\nu_Q$ is measured, eq 2 has two solutions for values of the observed splitting $|\Delta\nu_Q| < \Delta\nu_Q^{\text{powder}}$, i.e., for angles between 35.3 and 90°. Strictly speaking, the constant $\Delta\nu_Q^{\text{powder}}$ may be positive or negative, but since only the frequency splitting is measured, we can define $\Delta\nu_Q^{\text{powder}}$ as being positive without loss of generality.

The purple membrane films used here are uniaxially oriented. The geometry of a single C−CD_3 bond with respect to the membrane normal **n** and the magnetic field $\mathbf{B_0}$ is depicted in Figure 2. Within one purple membrane, the bacteriorhodopsin molecules are immobilized and form trimers in a hexagonal lattice. Therefore, three different orientations for the specific C−CD_3 bond vector occur, all of which make the same angle γ with respect to the membrane normal indicated by the vector **n**. In the film, the membranes are stacked in parallel and rotated arbitrarily around **n** with respect to each other, such that the bond vectors lie on the rim of a cone with angle γ. To calculate the quadrupolar splitting from eq 2, we need to know cos θ, which equals $D_{00}^{(1)}(0,\theta,0)$, the Wigner matrix element of rank 1. Each individual bond in the uniaxially oriented sample is characterized by γ and the azimuthal angle ϕ which describes its position on the rim of the cone. The axis of the cone is inclined by the angle α'' away from the magnetic field. This geometry can be described by a two-step rotation from the bond to the cone axis **n**, and from the cone axis to the magnetic field. Using the transformation properties of the Wigner rotation matrixes, we can thus express $D_{00}^{(1)}(0,\theta,0)$ in the following way:

$$D_{00}^{(1)}(0,\theta,0) = \sum_{m=-1}^{1} D_{0m}^{(1)}(0,\gamma,\phi) D_{m0}^{(1)}(0,\alpha'',0) \qquad (3)$$

Inserting the matrix elements and simplifying leads to

$$\cos\theta = \cos\gamma\cos\alpha'' - \sin\gamma\sin\alpha''\cos\phi \qquad (4)$$

The situation is complicated by the fact that the membranes are not perfectly aligned, but the normals **n** are themselves distributed in space. This orientational disorder is called the mosaic spread. Assuming that the distribution of **n** is cylindrically symmetric around the average membrane normal $\bar{\mathbf{n}}$, we can use an expression analogous to eq 4 for the angle α'' between the local membrane normal **n** and the magnetic field (see Figure 2):

$$\cos\alpha'' = \cos\alpha'\cos\alpha - \sin\alpha'\sin\alpha\cos\phi' \qquad (5)$$

where α is the angle between the average membrane normal axis $\bar{\mathbf{n}}$ and the magnetic field $\mathbf{B_0}$, α' is the angle between the local membrane normal **n** and $\bar{\mathbf{n}}$, and ϕ' is the azimuthal angle of **n** on the cone with axis $\bar{\mathbf{n}}$.

In previous work, eq 4 was used to derive an analytical expression for the probability density $p(\nu)$ for one cone without mosaic spread (*41*). In the presence of orientational disorder, however, a comprehensive analysis of the geometry requires three transformations instead of two in eq 3. Moreover, since the quadrupolar splitting is given by the Wigner rotation matrix element $D_{00}^{(2)}(\Omega_{PL})$ of rank 2, the more detailed description of the sample geometry in analogy to membrane lipids (*42*) is given by

$$D_{00}^{(2)}(\Omega_{PL}) = \sum_{m',m=-2}^{2} D_{0m'}^{(2)}(\Omega_{PN}) D_{m'm}^{(2)}(\Omega_{ND}) D_{m0}^{(2)}(\Omega_{DL}) \qquad (6)$$

In the case of an axially symmetric field gradient, $\Omega_{PL} = (0,\theta,0)$ contains only the angle θ between the deuterated bond and the magnetic field. The first of the three rotations on the right-hand side of eq 6 with Euler angles $\Omega_{PN} = (0,\gamma,\phi)$ leads from the principal axis system of the residual electric field gradient to the local membrane normal **n**, the next one with $\Omega_{ND} = (0,\alpha',\phi')$ from the local membrane normal to the average membrane normal $\bar{\mathbf{n}}$, and the third one with $\Omega_{DL} = (0,\alpha,0)$ from the average normal to the magnetic field $\mathbf{B_0}$ in the laboratory system. In this case, the analytical expression for $p(\nu)$ contains elliptic integrals and becomes computationally cumbersome. If one does not wish to

analyze a given bond in the sample, but instead wishes to simply generate all possible bond orientations in the sample with an appropriate weighting factor, using eqs 4 and 5 is sufficient. Consequently, we have chosen a Monte Carlo-like approach to treat the mosaic spread problem as accurately as desired without complicating the mathematics unnecessarily. In this numerical procedure, angles α', ϕ', and ϕ, which describe the orientational and uniaxial distributions, are random variables, while the remaining angles α and γ are fixed parameters. By generating triple random values for α', ϕ', and ϕ and choosing α and γ, we calculate α'' using eq 5, insert this value into eq 4, and determine cos θ which in turn is used to calculate the corresponding quadrupolar splitting in eq 2. In this way, we accumulate a probability distribution of frequencies and simulate the line shape. To check whether our simplified but computationally much faster algorithm correctly reproduces the line shape, we have also programmed eq 6 with the rank 2 Wigner matrix elements. For 20 000 or more random triples, the line shapes generated in the two approaches are indistinguishable.

The angles ϕ and ϕ' are uniformly distributed from 0 to 2π. For the orientation of the local membrane normal, we assume a Gaussian probability distribution on the unit sphere, which means that α' is distributed in a Gaussian manner around 0° with a weighting factor of sin α'. This weighting factor is necessary for the Gaussian distribution of orientations in three-dimensional space to correspond to the distribution of angles α'. We therefore generate the corresponding cumulative distribution function $F(\alpha')$ according to

$$F(\alpha') = N\int_0^{\alpha'} \exp\left(\frac{-a^2}{2\sigma^2}\right) \sin a \, da \qquad (7)$$

where σ is the mosaic spread and N is a normalization constant such that $F(\pi) = 1$. For a random number F, uniformly distributed from 0 to 1, the corresponding value of α' is determined by numerically inverting the above equation. This is a general and standard method for the generation of nonuniformly distributed random numbers from uniformly distributed random numbers. It can be employed for arbitrary probability functions. If, for example, instead of a Gaussian probability density a constant probability density on the unit sphere is assumed, F is proportional to cos α', which leads to $\alpha' \propto \cos^{-1} F$. The resulting line shape is identical to the Pake powder pattern for an isotropic distribution of orientations. For polymer fibers, a Gaussian has been shown to be an adequate approximation (*43*), but more complex distributions can be analyzed with two-dimensional solid-state NMR (*44*).

The parameters of the simulation are the tilt angle α (average membrane normal) which is varied within ±3° of the set angle, the bond orientation (angle γ) which is obtained in a first approximation from the separation of the two maxima in the 0° tilt spectrum, the coupling constant $\Delta\nu_Q^{\text{powder}}$ which is determined from the powder-type spectrum, the line broadening which is also determined from the powder spectrum and an independent T_{2e} experiment, and the mosaic spread. All parameters except α are the same for each spectrum of a tilt series. The resulting line shape is then convoluted with a Lorentzian function, which represents the intrinsic line width due to spin−spin relaxation, as well as the exponential multiplication of 2 kHz applied to the echo. A total of 20 000 random triples are sufficient to result in a smooth and stable simulation after convolution. The simulated spectra also take into account the distortions due to the finite spectral width of the pulses (*45*). Calculation of a complete tilt series with seven spectra takes about 120 s on a desktop computer.

The Monte Carlo procedure for simulating the ^{2}H NMR line shape is a universally applicable tool for describing static line shapes. The derivation of a closed form solution for the probability density $p(\nu)$ is not required, but instead, the line shape is accumulated by randomizing the appropriate angles. It can easily be generalized by expanding the Wigner matrix elements $D^{(2)}_{m0}(\Omega_{PL})$ as in eq 6. In this way, line shapes can be calculated even in cases where the asymmetry parameter η_Q^{eff} is non-zero, as long as the geometry of the sample is known (*46*). Fixed angles are considered to be parameters of the model, and can be optimized by stepwise variation or automated searches of the parameter space.

It is apparent from Figure 2 that the set of angles θ corresponding to a given orientation of the bond angle cone depends on the tilt angle α as well as the bond angle γ. Thus, not only are the line shapes for different tilt angles different, but also those for different bond angles. A tilt series then allows one to differentiate the two solutions of eq 2 in cases where the observed separation of the two 0° tilt lines is less than $\Delta\nu_Q^{\text{powder}}$. We also note that eqs 4 and 5 can be easily derived without the formalism of the Wigner rotation matrixes, for example, using the scalar product of appropriate unit vectors in spherical polar coordinates. However, in general, the above formalism is more powerful and indispensable for more complex problems.

RESULTS

Powder-Type Samples. To determine the quadrupolar coupling constant $\Delta\nu_Q^{\text{powder}}$ in eq 2, a powder-type spectrum from purple membranes with the (1*R*)-1-CD_3-labeled retinal was measured at −50 and 20 °C. This sample contained only 45 mg of protein, but a relatively large amount of water. Residual deuterium in highly mobile water molecules leads to a strong broad peak at the Larmor frequency in the ^{2}H NMR spectrum, and a precise line shape analysis is very difficult. To suppress this signal, the sample was frozen at −50 °C. The water molecules are immobilized, and their deuterium signal leads only to a weak background, because the frequency range for a deuteron in ice is more than 3 times larger than that of the methyl rotor in the fast motional limit. The resulting ^{2}H NMR spectrum at −50 °C (Figure 3a) has a very good signal-to-noise level, which is clearly worse in the spectrum obtained at room temperature (Figure 3b). For the latter experiment, the sample had to be dried for many days to remove the water whose signal otherwise dominates the spectrum. The powder-type line shapes at low temperatures as well as at room temperature have been simulated using the analytical expression for the Pake pattern (*16*, *17*). The parameters are the constant $\Delta\nu_Q^{\text{powder}}$ and a Lorentzian line broadening. The $\Delta\nu_Q^{\text{powder}}$ values of the best simulation are 39.8 kHz at −50 °C and 38.8 kHz at 20 °C, with a line broadening of 3.4 and 3.3 kHz, respectively. Since the applied exponential multiplication was 2 kHz, the

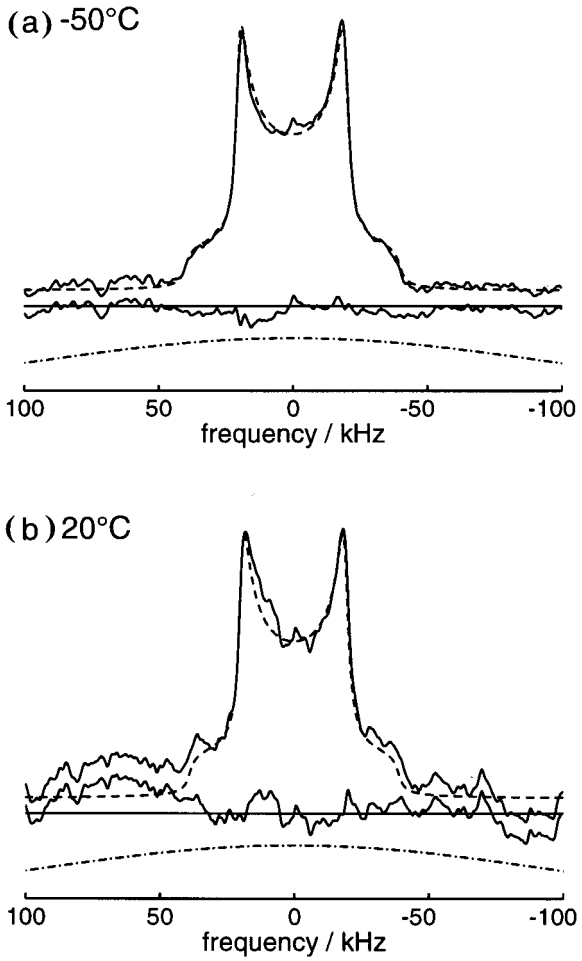

FIGURE 3: Powder-type ^{2}H NMR spectra of randomly oriented purple membranes containing bacteriorhodopsin with the (1*R*)-1-CD_3-labeled retinal: (a) −50 °C, 350 000 scans, and a recycle time of 200 ms (—) and (b) 20 °C, 320 000 echos, and a recycle time of 500 ms (—). Superposed in each part is a simulation of the Pake powder pattern (- - -) for a symmetric coupling tensor (*16*). Below the powder pattern, the residuals between fit and data are shown. The fitting parameters are the quadrupolar coupling constant $\Delta\nu_Q^{\text{powder}}$ corresponding to values of 39.8 kHz at −50 °C and 38.8 kHz at 20 °C and a Lorentzian line broadening of 3.4 kHz at −50 °C and 3.3 kHz at 20 °C. The power spectrum of the 90° pulse (− • −) was calculated as described in ref *45* for a pulse length of 3.2 μs and is included in the simulated line shape.

intrinsic line width must be on the order of 1−1.5 kHz, assuming Lorentzian broadening.

Since the signal strength due to only three deuterons per protein is very low, we checked whether spurious signals from natural abundance deuterium distort the spectrum. A control powder-type sample of purple membranes was prepared in exactly the same way as the labeled sample, except that it contained a fully protonated retinal, and was measured under identical conditions. At −50 °C, the resulting ^{2}H NMR spectrum was indistinguishable from the baseline (data not shown), resembling the residuals in Figure 3, while at room temperature, only one narrow line at the carrier frequency was observed, corresponding to residual deuterium in water.

To further reduce the number of free parameters in the fits of the line shapes for the oriented sample, we determined T_{2e} by varying the pulse delay from 40 to 320 μs. The latter corresponds to a time-to-echo delay of about 650 μs, at which

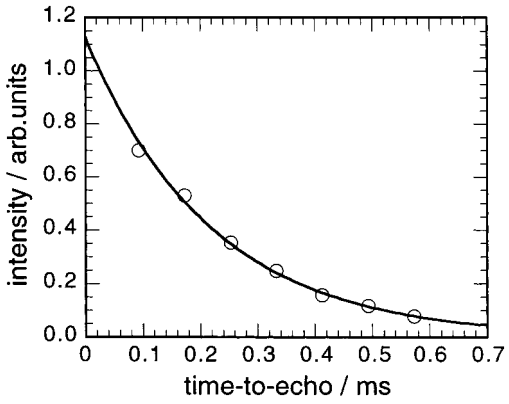

FIGURE 4: Determination of the decay T_{2e} of the quadrupolar echo for the (1*R*)-1-CD_3-labeled sample at 20 °C. The quadrupolar echo from the oriented sample was recorded at 0° tilt for seven different pulse delays. After Fourier transformation, the lines were fitted and the integral was plotted as a function of the time-to-echo delay, which is the sum of the delays after the first and second pulse plus the length of one pulse. An exponential fit of the decay gives a rate of 5.1 × 10^3 rad/s, corresponding to a Lorentzian line broadening of 1.6 kHz.

no quadrupolar echo was discernible from the noise level. In this experiment, we used the oriented sample at 0° tilt. The integrated intensity as a function of the time-to-echo delay is plotted in Figure 4. An exponential fit gives a time constant T_{2e} of 195 μs, which corresponds to a line broadening of 1.6 kHz and is consistent with the above estimate. Because a 2 kHz exponential multiplication was applied to the quadrupolar echo, we have used a total Lorentzian line broadening in the fits of the oriented line shapes of 3.5 ± 0.5 kHz.

Oriented Sample: Tilt Series. For a perfectly uniaxially oriented sample, the angle γ the C_1-CD_3 bond makes with the local membrane normal is identical to the angle θ the bond makes with the magnetic field at the 0° tilt orientation, where the membrane normal and the magnetic field are aligned. The resulting ^{2}H NMR spectrum consists of two lines whose separation corresponds to θ according to eq 2. The orientational disorder of the membrane normals broadens these two lines inhomogeneously. The experimental spectrum recorded at 20 °C is shown in the bottom row of Figure 5 for 0° tilt. The separation of the maxima of the two broad lines is ca. 26 kHz, which together with the constant $\Delta\nu_Q^{\text{powder}}$ corresponds to θ angles of either 70 or 42°, where for the former solution a negative splitting is assumed and for the latter a positive one. To not only differentiate the two solutions but also determine the angle more accurately, a tilt series of seven spectra was recorded by varying the sample inclination from 0 to 90° in steps of 15°. The whole series was fitted simultaneously with one set of parameters. The value of the constant $\Delta\nu_Q^{\text{powder}}$ was allowed to vary within 0.5 kHz of 39.3 kHz, the intrinsic line width plus exponential multiplication within 0.5 kHz of 3.5 kHz, and the tilt angle within 3° of the set angle. The mosaic spread and the bond orientation γ were free parameters.

The tilt series simulations for both solutions of the bond angle at 20 °C are presented in the left- and right-hand columns of Figure 5. The right-hand column shows the excellent agreement with the data for a bond orientation of 68.8°, as can be seen from the residuals plotted below each experimental spectrum. The small peak in the middle arises

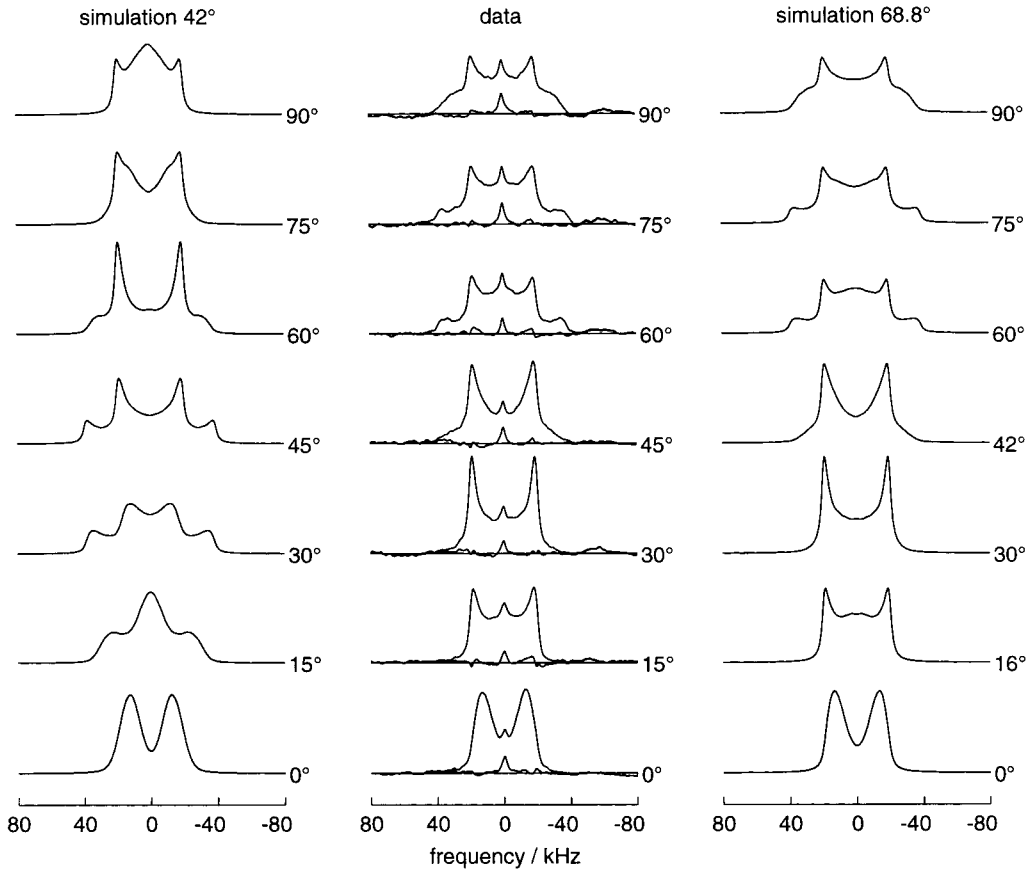

FIGURE 5: Experimental ^{2}H NMR tilt series at 20 °C and spectral simulation for the (1*R*)-1-CD_3-labeled bR. The data sets are the sum of two independent experiments of 350 000 acquisitions each with tilt angles of ≥30°, three experiments with a tilt angle of 15°, and five experiments with 0° tilt. The right panel shows the best fit simulation using a C−CD_3 bond angle γ of 68.8°. The left panel shows the corresponding simulations for the other solution of eq 2 which do not describe the data at all. In this case, the bond angle γ value of 42° and mosaic spread σ value of 5.2° were chosen such that the 0° tilt data are fit best. All simulated spectra take into account spectral distortions due to the finite pulse width (*45*). The middle panel depicts the ^{2}H NMR data, and below them, the residuals indicate the difference from the fits in the right-hand column. Next to the data are the values for the set tilt angle, and next to the simulated curves are the tilt angles used in the calculation. A deviation of up to 3° from the set angle was allowed for the tilt angles. The fit parameters are summarized in Table 1.

most likely from natural abundance deuterium in water. The theoretical spectra in the left-hand column were generated by using the smaller angle solution of 42° and fitting the 0° lines. The resulting set of parameters was used to calculate the line shape at each tilt, and it is obvious that no fit was achieved. It should be noted that the mosaic spread for the small angle solution is less than that for the fit with the larger bond angle, 5.2 versus 7.2°, respectively. This is due to the larger slope of the P_2 Legendre polynomial around 42° than at 70°, resulting in a larger change in splitting for a given variation of the sample inclination.

The same experiment was also performed at −50 °C to check whether motion influences the line shape. The resulting tilt series and its fit are shown in Figure 6. The peak at the carrier frequency has vanished as in the case of the powder-type sample at −50 °C, but otherwise, the spectra are identical to those at room temperature. The fit parameters for the low-temperature as well as for the room-temperature experiments are summarized in Table 1. The simulation is very sensitive to the bond orientation, which is highly correlated with the quadrupolar coupling constant, however. The error of the determined angle can therefore only be estimated to be about 2°.

The mosaic spread σ values of ±7.2° at 20 °C and ±8.7° at −50 °C obtained from the simulations are only slightly larger than that determined from lamellar diffraction experiments performed on similarly prepared samples (*2*). It is important to note that while the mosaic spread is defined for the angle α' and is therefore a property of the sample, the distribution of α'' in the laboratory system depends on the tilt angle α. While the membrane normals are distributed in a Gaussian manner in the frame of the average normal, it is not so in the laboratory frame. Therefore, in the case of a uniaxial distribution, it is incorrect to simply add a Gaussian weighted series of subspectra at varying tilt angles.

Table 1: Parameters for Best Fit Line Shape Simulations of (1*R*)-1-CD_3-Labeled Oriented Purple Membranes[a]

	20 °C	−50 °C
bond angle γ (deg)	68.8	68.6
mosaic spread σ (deg)	±7.2	±8.7
line broadening (kHz)	3.2	3.4
$\Delta\nu_Q^{powder}$ (kHz)	39.3	39.7

[a] The tabulated parameters were used to simulate the line shapes in Figures 5 and 6 for a complete tilt series at the given temperatures, varying only the tilt angle for different data sets. The simulations use a frequency grid of 1024 points, where 20 000 random triples are sufficient for the generation of one spectrum.

Retinal Orientation from Combined Analysis of Deuterium NMR, Linear Dichroism, and Electron Microscopy Data.

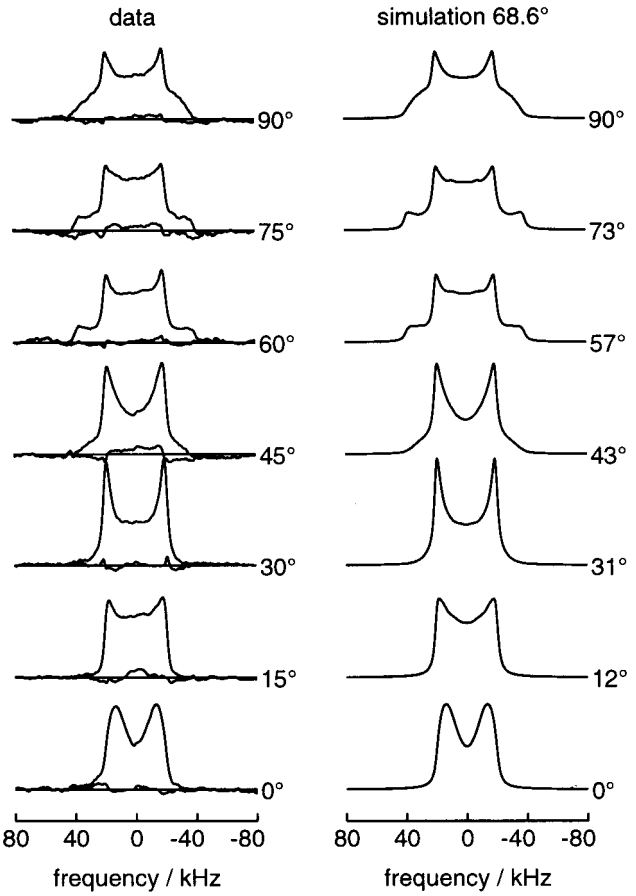

FIGURE 6: Experimental ^{2}H NMR tilt series and spectral simulations for (1*R*)-1-CD_3-labeled bR at −50 °C. All spectra (data as well as simulations) have been scaled such that their integral is the same. The data in the left panel represent 250 000 acquisitions each and their deviation from the fit, which is shown in the right panel. The angles next to the spectra refer to the set angle for the data and the angle used in the simulation, respectively. A deviation of up to 3° from the set tilt angle was allowed in the simulation. All simulated spectra take into account spectral distortions due to the finite pulse width (*45*). A summary of the fit parameters is given in Table 1.

One aim of this study was to find restrictions for the possible orientations of the chromophore within the membrane. In general, three angles are sufficient to fix the position of a rigid body in space. In the case of the retinal chromophore, only two angles are needed because one can consider the membrane a uniaxial system, and therefore, the third angle may have an arbitrary value. This geometrical problem can again be formulated using Wigner rotation matrices. In the simplest case, one has to relate the angle determined by ^{2}H NMR to the molecular frame and the latter to the membrane frame

$$D^{(j)}_{00}(\Omega_{PN}) = \sum_{m'=-j}^{j} D^{(j)}_{0m'}(\Omega_{PM}) D^{(j)}_{m'0}(\Omega_{MN}) \qquad (8)$$

where $\Omega_{PN} = (0,\beta_{PN},0)$ represents the bond angle obtained from ^{2}H NMR, $\Omega_{PM} = (0,\beta_{PM},\gamma_{PM})$ are the Euler angles for the rotation from the principal axis system of the bond to the chosen molecular frame of the retinal, and finally $\Omega_{MN} = (\alpha_{MN},\beta_{MN},0)$ are the two angles for the rotation of the molecular to the membrane frame. The angles α_{MN} and β_{MN} describe the orientation of the retinal in the frame of the membrane, whereas the angles Ω_{PM} can be determined from

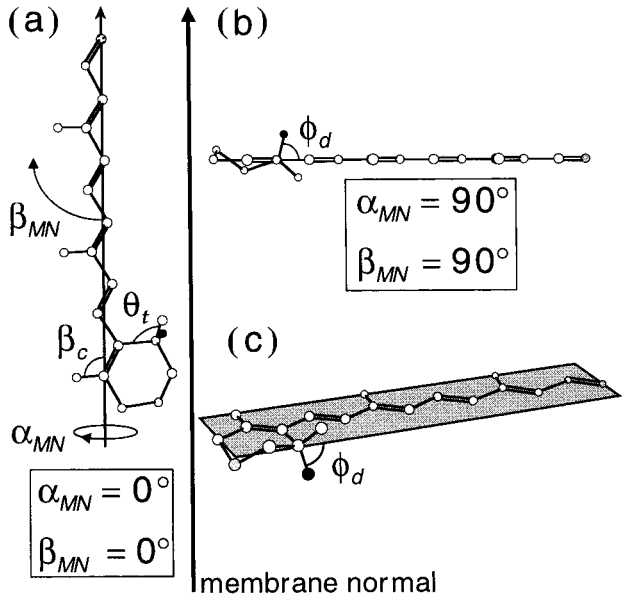

FIGURE 7: Modeling of chromophore orientation in the purple membrane. The orientation of the retinylidene chromophore with respect to the membrane is determined by two angles α_{MN} and β_{MN}. The polyene chain is defined as the vector from C_5 on the cyclohexene ring to the Schiff base nitrogen, which is the last atom of the chain drawn here. Thus, β_{MN} is the tilt angle between the polyene chain vector and the membrane normal, whereas the ring plane roll α_{MN} is a rotation around the chain vector. The intramolecular angles characterizing the configuration of the cyclohexene ring are θ_t and ϕ_d. The tetrahedral angle θ_t involves the sp^3 hybridized orbitals of C_1 and is the same for all bonds on C_1. The dihedral angle ϕ_d of the (1*R*)-1-CD_3 bond is defined with respect to the C_6-C_1 bond and the ring plane. It depends on the type of half-chair conformation involving C_3 and C_2. The ring puckering (twisted half-chair) is clearly seen in panels b and c. For the sake of simplicity, the retinal is depicted as completely planar between C_4 and C_{15}, including the methyl groups attached to the polyene chain and C_5. The angle β_c is the angle between the polyene chain vector and the C_5-Me bond. The three panels are drawn for three different pairs of α_{MN} and β_{MN}. In panel a, both angles are set to 0° so that the chain vector is parallel to the membrane normal and the ring plane is perpendicular to the membrane surface ($\alpha_{MN} = 0°$ and $\beta_{MN} = 0°$). Panel b is a view from above onto the retinal, with the methyl groups of the polyene chain pointing out of the paper plane ($\alpha_{MN} = 90°$ and $\beta_{MN} = 90°$). Panel c is an illustration of an arbitrary pair of angles α_{MN} and β_{MN}.

the conformation of the retinal molecule. The above eq 8 is valid for any rank *j*. In the case of ^{2}H NMR, the rank is 2, but a formulation in rank 1, which is computationally much easier to handle, is still correct if we take into account that in rank 2 we cannot distinguish the Euler angles $(\alpha,\beta,0)$ from $(\alpha+\pi,\pi-\beta,0)$, because even rank expressions are invariant under an inversion operation.

The most convenient choice for the molecular frame *M* is the long axis of the retinylidene polyene chain (C_5-N) as the *z*-axis, because in this case the Euler angle α_{MN} is the ring plane roll and β_{MN} is the tilt of the polyene chain with respect to the membrane normal. Both of them can be related to experimentally obtained values, i.e., the dichroism of the HOOP modes in FTIR and the dichroism of the electronic transition dipole moment. Because eq 8 contains two unknowns, viz. α_{MN} and β_{MN}, we must combine two such equations to be able to solve them for α_{MN} and β_{MN}. Thus, our analysis proceeds in three steps. First, we use the orientation of two bonds determined from ^{2}H NMR and their relative orientation given by the retinal conformation and

calculate the polyene chain tilt β_{MN} and ring plane roll α_{MN} in the membrane frame. We then select those solutions with a polyene chain tilt compatible with a transition dipole moment tilt of $70 \pm 5°$ with respect to the membrane normal. In the last step of our analysis, we take into consideration the fact that the vector from the cyclohexene ring to the Schiff base points toward the cytoplasmic side. This side-specific orientation allows us to classify the solutions with respect to the orientation of the Schiff base N−H bond, including whether it points toward the extracellular or cytoplasmic side of the membrane. For all solutions, we also have to take into account those corresponding to an inversion of the system.

If only one bond orientation for the retinal is known from ^{2}H NMR, e.g., the angle between the C_5−Me and the membrane normal, the only conclusion is that this bond lies anywhere on a cone pointing either to the extracellular or to the cytoplasmic side of the membrane, because with ^{2}H NMR one cannot distinguish an angle θ from its supplement $\pi - \theta$. Two such angles further restrict the possible orientations if the relative orientation of the two bonds is known. For the methyl groups along the polyene chain, the relative orientations are not known, because the chain may be bent and twisted. We have therefore chosen the orientation of the C_1−(1*R*)-CD_3 bond ($\gamma_1 = 68.7°$) together with that of the C_5−Me bond ($\gamma_2 = 37°$) investigated in previous work (*21*). The geometry of the cyclohexene ring defines the relative orientation of these two groups. The ring is planar between C_1, C_6, C_5 (and its methyl group), and C_4, while either C_3 is out of plane (half-chair) or both C_2 and C_3 assume one of two possible twisted half-chair conformations. These two conformations lead to different orientations of the labeled methyl group on C_1 with respect to the ring plane, characterized by the dihedral angle of the C_1−CD_3 bond about the C_1−C_6 bond (cf. Figure 7). We define β_{MN} as the angle between the polyene chain vector from C_5 to the Schiff base nitrogen (molecular principal axis) and the membrane normal, and α_{MN} as the roll of the ring plane around the chain vector. We expand the two known bond orientations, i.e., the angles between these bonds and the membrane normal, by using Wigner rotation matrices as described above:

$$\cos \gamma_2 = D^{(1)}_{00}(\Omega_{PN}) = \sum_{m=-1}^{1} D^{(1)}_{0m}(\Omega_{PM}) D^{(1)}_{m0}(\Omega_{MN}) \quad (9)$$

$$\cos \gamma_1 = D^{(1)}_{00}(\Omega_{P'N}) = \sum_{m',m=-1}^{1} D^{(1)}_{0m'}(\Omega_{P'P}) D^{(1)}_{m'm}(\Omega_{PM}) D^{(1)}_{m0}(\Omega_{MN}) \quad (10)$$

For both equations, the initial *z*-axis is aligned with the respective C−C bond. Of the three Euler angles, the first one is a rotation around this *z*-axis, the second one a rotation around the new *y*-axis, and the third one a rotation around the new *z*-axis. Thus, in eq 9, the C_5−Me bond (*z*-axis) is rotated through $\Omega_{PM} = (0,\beta_c,0)$ around the *y*-axis, which is perpendicular to the ring plane, onto the chain vector connecting C_5 with the Schiff base nitrogen. With the next transformation $\Omega_{MN} = (\alpha_{MN},\beta_{MN},0)$, the new *y*-axis is first aligned with the membrane plane (α_{MN}), and subsequently, the C_5−N vector is rotated through β_{MN} such that it is parallel to the membrane normal. In eq 10, the initial set of Euler angles $\Omega_{P'P} = (0,\theta_t,-\phi_d)$ aligns the principal axis system associated with the C_1−CD_3 bond with that of the C_5−Me bond. First, the *z*-axis C_1−(1*R*)-CD_3 is rotated around the *y*-axis through the tetrahedral angle θ_t onto the C_1−C_6 direction. Since this *y*-axis is also perpendicular to the original C_1−CD_3 axis, which makes an angle ϕ_d with the ring plane, we now rotate around the C_1−C_6 bond (new *z*-axis) by $-\phi_d$ so that the *y*-axis is now perpendicular to the ring plane. The remaining rotations in eq 10 are the same as in eq 9. The above transformations define as $\beta_{MN} = 0$ the retinal orientation in which the C_5−N vector points up along the membrane normal, and $\alpha_{MN} = 0$ as that in which the ring plane is perpendicular to the membrane plane. An illustration of the above-defined angles can be found in Figure 7. It should be noted that our formulation uses the notation for passive rotations of the coordinate systems.

Since the angles γ_1 and γ_2 were determined experimentally, eqs 9 and 10 can be solved for the two unknowns, cos β_{MN} and cos α_{MN}:

$$\cos \beta_{MN} = \frac{1}{\sin \theta_t}\Big\{[\sin \theta_t \cos \beta_c \cos \gamma_2 - (\cos \gamma_1 - \cos \gamma_2 \cos \theta_t) \sin \phi_d \sin \beta_c] \pm \cos \phi_d \sin \beta_c \times \sqrt{[\cos(\gamma_1 - \gamma_2) - \cos \theta_t][\cos \theta_t - \cos(\gamma_1 + \gamma_2)]}\Big\} \quad (11)$$

$$\cos \alpha_{MN} = \frac{\cos \beta_c \cos \beta_{MN} - \cos \gamma_2}{\sin \beta_c \sin \beta_{MN}} \quad (12)$$

In general, the two solutions of the quadratic equation are different and not related by an inversion with respect to the membrane plane. The square root is real only if $|\gamma_1 - \gamma_2| \leq \theta_t = 109° \leq (\gamma_1 + \gamma_2)$. In our case, $\gamma_1 + \gamma_2 = 68.7° + 37°$ which does not satisfy the above inequality. We can therefore conclude that one of the angles must be $180° - \gamma_i$, which is consistent with the NMR experiment in which only $|\cos \gamma_i|$ is determined. This means that the two bonds point toward opposite sides of the membrane. If one or both angles are a little larger, however, this conclusion does not hold. Since the quadrupolar interaction is invariant under an inversion, it is important to note that the square root is invariant with respect to this operation.

Equations 9 and 10 combine the information about the internal retinal conformation with the ^{2}H NMR information about the bond orientations with respect to the membrane normal. The angles θ_t, ϕ_d, and β_c characterize the intramolecular structure of the retinal molecule, while angles γ_1 and γ_2 describe the orientation of individual bonds with respect to the membrane normal. Using these five angles as input, one can then use eqs 11 and 12 to calculate the chain tilt β_{MN} and the ring plane roll α_{MN}, which define the retinal ring orientation with respect to the membrane plane. The internal chromophore conformation in bR is of course not known. We have therefore taken the values of the dihedral angle ϕ_d as well as β_c from two different structures, namely, from the retinal structure as determined by ideal orbital hybridization and from the crystal structure of the all-trans-6-s-trans-retinal model compound *N*-methyl-*N*-phenylretinal iminium perchlorate (*4*) which has a protonated Schiff base. Moreover, we have considered several possible types of ring puckering.

Table 2: Retinal Orientation in the Membrane Frame Deduced from ^{2}H NMR for Different Ring Conformations[a]

retinal structure	ring pucker	solution no.	dihedral angle ϕ_d (deg)	plane roll α_{MN} (deg)	chain tilt β_{MN} (deg)
ideal orbital	half-chair	1	59.5	25 (26)	66 (63)
geometry, $\beta_c = 94°$ (90°)		2	59.5	16 (15)	128 (124)
	twisted half-chair	3	42	32 (32)	75 (71)
		4	42	25 (25)	122 (118)
		5	77	16 (16)	60 (56)
		6	77	2 (2)	131 (127)
N-methyl-*N*-phenylretinal iminium	twisted half-chair	7	55 [(1*R*)-1-Me]	24 (25)	71 (67)
		8	55 [(1*R*)-1-Me]	23 (22)	130 (127)
perchlorate, $\beta_c = 99°$ (95.5°)		9	68 [(1*S*)-1-Me]	20 (21)	67 (63)
		10	68 [(1*S*)-1-Me]	10 (10)	135 (131)

[a] The dihedral angles ϕ_d correspond to the different ring pucker conformations. The following definitions apply. The polyene chain vector connects C_5 with the Schiff base nitrogen. β_c is the angle between the C_5-Me bond and the polyene chain vector. The chain tilt β_{MN} is the angle between the polyene chain vector and the membrane normal, where the ring plane roll α_{MN} is a rotation around this vector. Angles in parentheses correspond to the C_5-C_{15} vector as a reference direction.

For the retinal structure as determined by ideal orbital geometry, the angles describing the intramolecular conformation can easily be derived by trigonometric means. The cyclohexene ring of the retinal can exist in several conformations. In the simplest half-chair conformation, all carbons of the cyclohexene ring but C_3 are planar and the two geminal methyl groups on C_1 are symmetric with respect to this plane. The dihedral angle ϕ_d equals 59.5°. More realistic is a twisted half-chair conformation in which the two methyl groups on C_1 are positioned asymmetrically with respect to the ring plane defined by C_1, C_6, C_5, and C_4. They form different angles ϕ_d with the ring plane in these two conformations. For each of the two forms, there are two possible chain tilt angles β_{MN} from eq 11 with corresponding plane roll angles α_{MN} from eq 12. The values for ϕ_d in the two twisted half-chair conformations are 42 and 77°, respectively. The geometry of the bonds of C_1 is tetrahedral, and θ_t equals 109.5°. The C_5-Me bond makes an angle β_c of 94° with the C_5-N vector, but is at right angles to the C_5-C_{15} direction.

In the case of the crystal structure of the retinal model compound *N*-methyl-*N*-phenylretinal iminium perchlorate, all angles can be calculated from the atomic coordinates (*4*). The ring, however, was found in only one pucker conformation. As an approximation for the two twisted half-chair conformations, we use as input either one of the dihedral angles of the two methyl groups on C_1 and their respective tetrahedral angles: $\theta_t = 113°$ and $\phi_d = 55°$ for the C_1-(1*R*)-Me and $\theta_t = 110°$ and $\phi_d = 68°$ for the C_1-(1*S*)-Me bonds, respectively. The angle β_c between the C_5-Me bond and the C_5-N chain direction is found to be 99°, whereas the angle with respect to the C_5-C_{15} vector is 95.5°. The results for the two retinal models and their ring pucker conformations are summarized in Table 2. An illustration of one pair of solutions for the retinal model compound is presented in Figure 8.

The local orientation of the plane of the polyene chain of the chromophore has been obtained previously from polarized FTIR measurements on the hydrogen-out-of-plane (HOOP) vibrations (*33*, *47*, *48*). Experiments on the $C_7{=}C_8$ and $C_{11}{=}C_{12}$ HOOP modes have shown that these local planes are approximately perpendicular to the plane of the membrane (±10°), but that small twists of 15−30° occur around single bonds. These results thus suggest that a tilt of the ring plane of up to 20 or 30° is not unreasonable. Consequently, they do not provide a constraint for distinguishing the various structures found in the modeling described above, because all ring plane roll angles in Table 2 are less than 32°. However, the orientation of the optical transition dipole moment at 568 nm with respect to the membrane normal is known with good precision to be 70 ± 5° (*30*, *31*, *33*). The orientation of the C_5-N vector is close to that of the transition dipole moment in either the all-trans or 13-cis form (*49*, *50*), and thus provides an additional orientational constraint for the polyene chain (cf. Figure 8). Because the transition dipole moment and the above-defined vector nevertheless may differ somewhat, we use as a selection criterion the fact that the polyene chain tilt must lie in the interval of 70 ± 10°. Clearly, only solutions 1, 3, 5, 7, and 9 of Table 2 satisfy this criterion, because a tilt angle of, for example, 130° corresponds to 50°. If the C_5-C_{15} vector is used as a reference direction, β_c is about 4° smaller and the numbers in parentheses in Table 2 show that this difference is directly seen in the corresponding chain tilt β_{MN} which also changes by about 4°. This is understandable, because the plane is nearly perpendicular to the membrane plane ($\alpha_{MN} \leq 30°$). Considering the case of a 13-cis chromophore, β_c would be larger than in the all-trans form and the chain tilt angles would increase by approximately the same amount. This means that for solutions 2, 4, 6, 8, and 10 in Table 2 the chain tilt would be even further removed from the value of 110°, which corresponds to the 70° inclination of the transition dipole moment. Thus, the conclusion that only the odd-numbered solutions in Table 2 are compatible with the linear dichroism experiment holds in all of the above cases.

As a final step of our analysis, we investigate the orientation of the methyl groups and the Schiff base N−H bond within the membrane frame. It follows from our definition of the rotations that for a solution with a chain tilt β_{MN} of less than 90° and a ring plane roll α_{MN} between 90 and −90°, the polyene methyls point toward the side of the membrane to which the C_5-N vector points. Clearly, this is the case for all configurations compatible with the linear dichroism experiments (solutions 1, 3, 5, 7, and 9 in Table 2). Also, it is known from electron microscopy (*3*) and second-harmonic interference experiments (*32*) that the C_5-N vector points toward the cytoplasmic side of the membrane. Therefore, we can conclude that the polyene methyl groups point toward the cytoplasmic side and the Schiff base N−H bond points toward the extracellular side of the membrane. The opposite orientation can be excluded

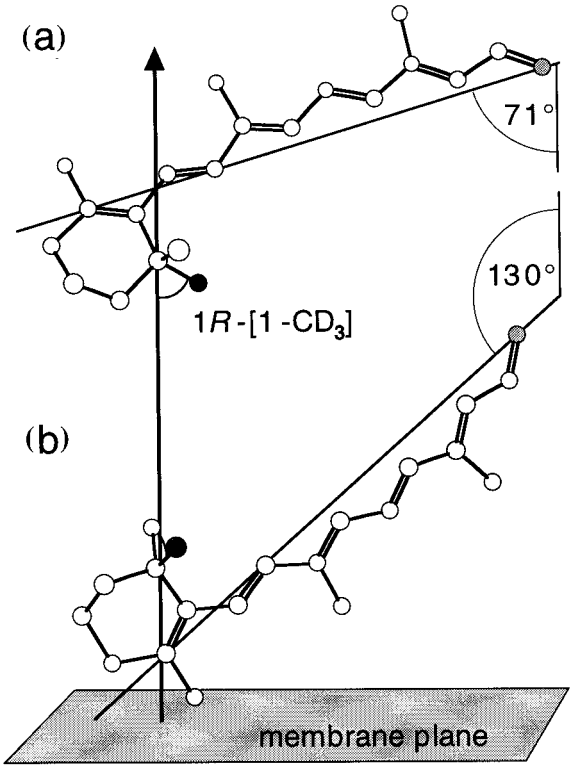

FIGURE 8: Three-dimensional rendering of two orientations of the retinal in the membrane as derived from orientational constraints. The atomic coordinates for the carbon atoms and the Schiff base nitrogen (last atom of the chain) were taken from the crystallographic structure of the all-trans-6-s-trans-retinal model compound *N*-methyl-*N*-phenylretinal iminium perchlorate (*4*). The carbon atom of the deuterated (1*R*)-1-CD_3 methyl group studied in this work is black (ϕ_d = 55°). Orientations a and b correspond to the two solutions resulting from the constraints on the bond orientations for the C_5−Me and (1*R*)-1-CD_3. For ease of comparison, the drawing of the chromophore in part b is inverted such that the deuterated methyl group lies behind the paper plane in part a and in front of it in part b. Clearly, the inclination of the polyene chain vector connecting C_5 on the ring with the nitrogen at the Schiff base end relative to the membrane normal is different in the two configurations. The numerical values for the chain tilt are indicated in the figure; the corresponding plane roll can be found in Table 2 (solutions 7 and 8). Only the tilt of 71° in part a is consistent with previous results from linear dichroism studies. Since it is known that the cyclohexene ring is closer to the extracellular side, the configuration consistent with both constraints in part a has the polyene methyls pointing toward the cytoplasmic side and the Schiff base N−H bond pointing toward the extracellular side. For a detailed explanation, see the text.

because the polyene chain tilt would not be consistent with the results from linear dichroism (solutions 2, 4, 6, 8, and 10 in Table 2). It is well-known that the quadrupolar interaction as well as linear dichroism are insensitive to a change in angle from θ to 180° − θ. Our conclusion is independent of this restriction, because if we change the angles γ_1 and γ_2 to 180° − γ_1 and 180° − γ_2, respectively, cos β_{MN} changes its sign in eq 11; i.e., β_{MN} is also replaced by 180° − β_{MN}. The same holds for α_{MN} in eq 12. It should be noted that the angles defining the intramolecular conformation of the retinal remain unchanged under the inversion, and the root in eq 11 must still be real, i.e., $\gamma_1 + \gamma_2 > 109°$. Thus, the inversion leaves our conclusion unaltered, because the membrane reference system as a whole is inverted. It follows that the orientation of the retinal within the membrane frame is unchanged and the Schiff base N−H bond still points toward the extracellular side. This can be done experimentally by turning the sample by 180° which results in the same quadrupolar splitting. It is the combination of three angles, from ^{2}H NMR and linear dichroism, with a defined retinal structure and the orientation information from electron microscopy that makes our conclusion unambiguous.

DISCUSSION

For understanding the mechanism of proton translocation by bacteriorhodopsin (bR) in the purple membrane, knowledge of the structure of the retinal chromophore and its orientation is centrally important. The angular constraints provided by ^{2}H NMR spectroscopy are valuable in this regard, particularly in combination with complementary biophysical approaches, such as linear dichroism, electron cryomicroscopy, and nonlinear optical interference measurements. The wide-line ^{2}H NMR experiments described in this article were performed on a uniaxially oriented sample of hydrated purple membranes containing bacteriorhodopsin with a (1*R*)-1-CD_3-labeled retinal. For the first time, ^{2}H NMR spectra with a high signal-to-noise ratio could be collected not only at sub-zero temperatures but also at room temperature (20 °C). Thus, in contrast to electron cryomicroscopy (*29*), our experiments have been performed under conditions close to those for the native system.

The width of the Pake powder pattern of a random dispersion of purple membranes at 20 °C does not change significantly upon lowering the temperature to −50 °C, which is consistent with previous studies on the methyl rotor dynamics in bR (*27*). Since the average powder splitting of 39.3 kHz is very close to the expected value of $\Delta\nu_Q^{\text{powder}} = {}^1/_3({}^3/_4\chi_Q^{\text{stat}}) \simeq {}^1/_4(170)$ kHz for a methyl rotor in the fast motional limit (*27*), no additional fast motions with rates $\geq 10^4$ s^{-1} seem to be present. In the case of the oriented sample, experiments were performed at 20 and −50 °C. Again, no significant differences were observed which suggests that dynamical differences over this temperature range do not affect the line shape. This may indicate that there are no significant dynamical contributions from ring puckering. On the other hand, ring puckering may be so slow as to lead to two overlapping sets of lines. This possibility cannot be ruled out with certainty, because the bond angles with respect to the membrane differ by only a few degrees in the two twisted half-chair conformations.

Angular Constraints from Deuterium NMR Spectroscopy of Isotopically Labeled Retinal in Bacteriorhodopsin. In this work, the angle of the stereospecifically labeled methyl group on C_1 of the cyclohexene ring relative to the frame of the purple membrane was investigated. The quadrupolar interaction and consequently the observed quadrupolar splitting depend on the angle between the respective deuterated bond and the magnetic field (*16*). By orienting the sample in a defined way, we are able to deduce from the ^{2}H NMR experiment the angle between the bond and the orientational axis, in our case the membrane normal. Although a perfect orientation of the membranes is desirable and simplifies the analysis, a limited degree of orientational order is in fact sufficient to obtain useful information. The Monte Carlo procedure for simulating the deuterium line shape allows one to accurately take into account the disorder in the uniaxially aligned purple membrane films; no systematic differences

between the data and fit were observed. A tilt series of ^{2}H NMR spectra measured at seven different inclinations of the sample with respect to the magnetic field has been simultaneously analyzed with a common set of parameters. The tilt series not only allows one to distinguish the two bond orientations that are compatible with the observed splitting at zero sample tilt but also increases the precision with which the bond orientation is determined. Together with the known bond orientation for the methyl group on C_5 (*21*), this restricts the possible orientation of the planar part of the cyclohexene ring relative to the plane of the membrane.

In this study, the angle between the membrane normal and the C_1-CD_3 bond was found to be 68.7 ± 2.0°. The error is only an estimate and may even be smaller than 2°. This value is consistent with the angle of 67.4° derived from a refinement of electron crystallographic data (*3*) using the X-ray structure of a retinal model compound (*4*) as the starting point.[2] Because the bond orientations were calculated from atomic coordinates, they have large errors, whereas we achieve a precision of better than 2°. In a previous ^{2}H NMR study, values of 75 ± 2° and 94 ± 2° were reported for the orientations of the two geminal methyl groups of C_1 (*20*). The 75° value probably corresponds to the angle of 68.7 ± 2° found here. The reliability of the previous data analysis was limited, because all three methyl groups on the cyclohexene ring had been labeled (*20*). Hence, the corresponding three overlapping ^{2}H NMR spectra could not be deconvoluted properly. This problem was already recognized when the angle for the C_5-Me bond of 46° in ref *20* had to be revised to 37° in later work with a single specifically deuterated methyl group on C_5 (*21*).

For the C_5-, C_9-, and $C_{13}-$methyl bonds along the polyene chain, there are systematic deviations between the previous ^{2}H NMR results (*21*) and the values derived from electron cryomicroscopy (*3*) and X-ray diffraction (*5*). The angle between the C_5-methyl bond and the membrane normal obtained from ^{2}H NMR is 37° (*21*), from electron cryomicroscopy 39° (*3*), and from X-ray diffraction 32° (*5*) (all values rounded). Thus, for the C_5-methyl group, there is good agreement, considering the errors of ±2° in the NMR value and probably at least ±5° in the diffraction results. It should be noted that this angle was used in our determination of the chromophore orientation (see below). For the other methyl groups on C_9 and C_{13}, however, the corresponding values are 40, 29, and 34° and 32, 16, and 10° from ^{2}H NMR, electron microscopy, and X-ray diffraction, respectively, and there is clear disagreement. The angles from the diffraction experiments are systematically smaller than those from ^{2}H NMR with the discrepancy increasing toward the Schiff base end. The source of these differences remains unclear, because all experiments were presumably carried out with dark-adapted samples containing the same mixture of 13-cis and all-trans chromophores. The refinement of the diffraction structures was based, however, on the structure of an all-trans-retinal model compound (*4*). This choice would be inappropriate if significant differences existed in the methyl orientations in the 13-cis, 15-syn and the 13-trans, 15-anti chromophore isomers. Such differences may be largest near the end of the chain. If, for example, the Schiff base terminal part were twisted with respect to the average polyene plane, the ^{2}H NMR angle for the $C_{13}-$methyl bond orientation could be larger than the diffraction results, which are biased toward the nearly planar all-trans input structure. Also, the global *R* factor, a measure of the refinement of the entire protein structure, may not be very sensitive to the local structure of the chromophore whose scattering density is not very large. Another potential source of error lies in the definition of the membrane normal. The X-ray diffraction experiments were not carried out with purple membranes, and the direction of the membrane normal had to be taken over from electron cryomicroscopy.

Molecular Modeling of the Retinal Orientation in Bacteriorhodopsin. With regard to further modeling of the chromophore and integrating the ^{2}H NMR results in the framework of previously obtained data, two alternative strategies are possible. One can either combine the information from ^{2}H NMR with other constraints and try to deduce the structure of the chromophore or make assumptions about this structure to infer how the molecule as a whole is oriented with respect to the membrane. Here, we have chosen the latter approach, since the atomic structure of the chromophore in bR is not yet known. Thus, we have combined several pieces of evidence to build a model from which the possible orientations can then be calculated. One can expect that orientational constraints determined from ^{2}H NMR studies of the cyclohexene ring are dependent on its conformational puckering. To establish the generality and robustness of the conclusions, several conformations of the retinal and especially the ring puckering have been considered. These include the simplest half-chair ring conformation, in which only C_3 does not lie in the ring plane and the two methyl groups on C_1 are not affected by the puckering. A more realistic conformation is the twisted half-chair, in which both C_2 and C_3 are out-of-plane and the dihedral angle of the methyl groups on C_1 is different for the two possible conformations. As a further model for the retinal conformation in bR, we have used the crystallographically determined structure of *N*-methyl-*N*-phenylretinal iminium perchlorate (*4*). The results of our orientational analysis show that the conclusions about the retinal orientation with respect to the membrane are comparatively robust and do not depend on the detailed aspects of the ring puckering.

It is known from crystallographic studies on single crystals of the all-trans-retinal model compound (*4*) or all-trans-retinoic acid (*51*) that the molecule is planar to within 6° in the 6-s-trans configuration, while the 6-s-cis form shows a large twist between the polyene chain plane and the planar part of the ring of greater than 30° (*51, 52*). ^{13}C magic angle spinning experiments (*23*) as well as rotational resonance NMR studies (*25, 26*) have confirmed this observation, and have shown that the retinal in bacteriorhodopsin has a 6-s-trans configuration. Thus, the assumption in our calculations of a nearly planar retinal molecule including the polyene chain is very well-justified.

We have combined the result of the ^{2}H NMR experiments [(1*R*)-1-CD_3 bond] with the previously published angle for the C_5-Me bond from ^{2}H NMR (*21*) to determine orientational constraints for the plane of the cyclohexene ring in

[2] Grigorieff et al. (*3*) used a different nomenclature for the methyl groups. The angle of 67.4° is given in their Table 4 for the C_1-C_{17} methyl group. This methyl group is the one on the left side of the ring as seen from above (cf. their Figure 10) and thus corresponds to the (1*R*)-1-Me studied in this work (N. Grigorieff, personal communication).

the membrane. The calculations require as an input the dihedral angle ϕ_d for the (1*R*)-1-CD_3 bond around the C_1-C_6 bond. Data for ϕ_d vary considerably within 10−20° between crystal structures (*4*, *51*) and between crystallographic data and the ideal ring geometry calculated from sp^3 (tetrahedral) and sp^2 (trigonal) geometries. For each ring pucker conformer, two possible orientations of the retinal within the membrane are found. Each of them is characterized by the polyene chain tilt β_{MN} and a rotation α_{MN} around the polyene chain. From the total of 10 configurations, we select those in which the polyene chain tilt is compatible with the transition dipole moment orientation determined from linear dichroism studies, i.e., 65−75°. At this point, we are left with only four possible configurations. The tilt α_{MN} of the ring plane with respect to the membrane plane in the remaining structures is between 20 and 32°, and is consistent with the tilt of the planar parts of the polyene chain determined from the dichroism of the HOOP modes of the polyene chain, if the observed twists of 15−30° around the single bonds are taken into account (*33*, *47*, *48*). Moreover, since the vector from the cyclohexene ring to the Schiff base is known to be oriented toward the cytoplasmic side of the membrane (*29*), we can differentiate the two sides for the possible solutions. It turns out that in all four remaining solutions, the Schiff base N−H bond points toward the extracellular side of the membrane (cf. Results). This conclusion is not very sensitive to the values assumed for the angles involved in the calculation; e.g., in the case of the transition dipole moment inclination, we have allowed a 20° variation.

As a result, by combining the ^{2}H NMR data for two of the deuterated ring methyl groups, we have been able to further reduce the number of possible solutions for the orientation of the retinal in the membrane frame. The introduction of the orientation of the chain vector then links the retinal to the membrane frame. In this manner, it has been possible to overcome the inherent limitation of the ^{2}H NMR experiment, namely, that due to the even parity of the coupling interaction an angle θ cannot be distinguished from its supplement $\pi - \theta$. The conclusion that the Schiff base N−H bond points toward the extracellular side of the noncentrosymmetric membrane is thus not only unambiguous but also not very sensitive to the particular retinal conformation assumed, or to the particular orientation of the transition dipole moment.

Our conclusion regarding the retinal orientation within bR is consistent in its general features with the recent crystallographic findings (*5*). However, our calculations on the retinal orientation use only angles measured directly together with the retinal conformation, while in the input for a crystallographic refinement, a choice about the retinal orientation has to be made. Our conclusion is therefore independent and an interesting confirmation of the crystallographic results. The ^{2}H NMR experiments reported here measure bond orientations directly in the relevant frame of the native biomembrane. Analogous high-resolution NMR methods have been developed lately, which use directly measured angles to refine structures derived from distance or coordinate information (*53*). By combining the orientational information from ^{2}H NMR with X-ray studies of the entire protein, one may in the future be able to arrive at a detailed picture of the retinal binding pocket in bR.

Implications for the Molecular Mechanism of Ion Transport. Clearly, the orientation of the Schiff base N−H bond is an important element in vectorial proton transport. If the N−H bond points toward the extracellular side as concluded from our analysis, the proton points roughly toward aspartic acid 85, to which it is transferred in the L to M transition during the photocycle. However, in the M intermediate of the photocycle, the Schiff base still has an anti configuration, but the chromophore is in a 13-cis conformation, which may change the accessibility of the Schiff base to the cytoplasmic side and thus provide part of the switch mechanism. It will therefore be interesting to apply the method established in this work to the retinal in the M state once additional angles are determined using ^{2}H NMR spectroscopy. A detailed comparison of the structure and orientation of the chromophore before and after the switch will then be possible. Finally, we note that the methods applied here to the retinal chromophore in bacteriorhodopsin can also be applied to investigations of other ligands bound to membrane proteins, and may prove useful in the elucidation of their mechanism of action.

ACKNOWLEDGMENT

We thank Dr. Arnold Raitsimring for suggesting the Monte Carlo approach to line shape calculations. Help from Dr. Theodore Trouard and Jay Shumway with technical aspects of the NMR experiments is gratefully acknowledged.

REFERENCES

1. Heyn, M. P., Westerhausen, J., Wallat, I., and Seiff, F. (1988) *Proc. Natl. Acad. Sci. U.S.A. 85*, 2146−2150.
2. Hauss, T., Grzesiek, S., Otto, H., Westerhausen, J., and Heyn, M. P. (1990) *Biochemistry 29*, 4904−4913.
3. Grigorieff, N., Ceska, T. A., Downing, K. H., Baldwin, J. M., and Henderson, R. (1996) *J. Mol. Biol. 259*, 393−421.
4. Santarsiero, B. D., James, M. N. G., Mahendran, M., and Childs, R. F. (1990) *J. Am. Chem. Soc. 112*, 9416−9418.
5. Pebay-Peroula, E., Rummel, G., Rosenbusch, J. P., and Landau, E. M. (1997) *Science 277*, 1676−1681.
6. Krebs, M. P., Behrens, W., Mollaaghababa, R., Khorana, H. G., and Heyn, M. P. (1993) *Biochemistry 32*, 12830−12834.
7. Marassi, F. M., Ramamoorthy, A., and Opella, S. J. (1997) *Proc. Natl. Acad. Sci. U.S.A. 94*, 8551−8556.
8. Sefcik, M. D., Schaefer, J., Stejskal, E. O., McKay, R. A., Ellena, J. F., Dodd, S. W., and Brown, M. F. (1983) *Biochem. Biophys. Res. Commun. 114*, 1048−1055.
9. Stejskal, E. O., and Memory, J. D. (1994) *High-resolution NMR in the solid state: Fundamentals of CP/MAS*, Oxford University Press, London, U.K.
10. Sun, B. Q., Costa, P. R., Kocisko, D., Lansbury, P. T., Jr., and Griffin, R. G. (1994) *J. Chem. Phys. 102*, 702−707.
11. Lansbury, P. T., Jr., Costa, P. R., Griffiths, J. M., Simon, E. J., Auger, M., Halverson, K. J., Kocisko, D. A., Hendsch, Z. S., Ashburn, T. T., Spencer, R. G. S., Tidor, B., and Griffin, R. G. (1995) *Nat. Struct. Biol. 2*, 990−997.
12. Li, Y., Krekel, F., Ramilo, C. A., Amrhein, N., and Evans, J. N. (1995) *FEBS Lett. 377*, 208−212.
13. Goetz, J. M., and Schaefer, J. (1997) *J. Magn. Reson. 127*, 147−154.
14. Studelska, D. R., McDowell, L. M., Espe, M. P., Klug, C. A., and Schaefer, J. (1997) *Biochemistry 36*, 15555−15560.
15. Wang, J., Balazs, Y. S., and Thompson, L. K. (1997) *Biochemistry 36*, 1699−1703.
16. Seelig, J. (1977) *Q. Rev. Biophys. 10*, 353−415.
17. Brown, M. F. (1996) in *Biological Membranes* (Merz, K. M., Jr., and Roux, B., Eds.) pp 175−252, Birkhäuser, Secaucus, NJ.

18. Ketchem, R. R., Hu, W., and Cross, T. A. (1993) *Science 261*, 1457−1460.
19. Koeppe, R. E., II, Killian, J. A., and Greathouse, D. V. (1994) *Biophys. J. 66*, 14−24.
20. Ulrich, A. S., Heyn, M. P., and Watts, A. (1992) *Biochemistry 31*, 10390−10399.
21. Ulrich, A. S., Watts, A., Wallat, I., and Heyn, M. P. (1994) *Biochemistry 33*, 5370−5375.
22. Ulrich, A. S., Wallat, I., Heyn, M. P., and Watts, A. (1995) *Nat. Struct. Biol. 2*, 190−192.
23. Harbison, G. S., Smith, S. O., Pardoen, J. A., Courtin, J. M. L., Lugtenburg, J., Herzfeld, J., Mathies, R. A., and Griffin, R. G. (1985) *Biochemistry 24*, 6955−6962.
24. van der Steen, R., Biesheuvel, P. L., Mathies, R. A., and Lugtenburg, J. (1986) *J. Am. Chem. Soc. 108*, 6410−6411.
25. Creuzet, F., McDermott, A. E., Gebhard, R., van der Hoeff, K., Spijker-Assink, M. B., Herzfeld, J., Lugtenburg, J., Levitt, M. H., and Griffin, R. G. (1991) *Science 251*, 783−786.
26. McDermott, A. E., Creuzet, F., Gebhard, R., van der Hoef, K., Levitt, M. H., Herzfeld, J., Lugtenburg, J., and Griffin, R. G. (1994) *Biochemistry 33*, 6129−6136.
27. Copié, V., McDermott, A. E., Beshah, K., Williams, J. C., Spijker-Assink, M., Gebhard, R., Lugtenburg, J., Herzfeld, J., and Griffin, R. G. (1994) *Biochemistry 33*, 3280−3286.
28. Thompson, L. K., McDermott, A. E., Raap, J., van der Wielen, C. M., Lugtenburg, J., Herzfeld, J., and Griffin, R. G. (1992) *Biochemistry 31*, 7931−7938.
29. Henderson, R., Baldwin, J. M., Ceska, T. A., Zemlin, F., Beckmann, E., and Downing, K. H. (1990) *J. Mol. Biol. 213*, 899−929.
30. Heyn, M. P., Cherry, R. J., and Müller, U. (1977) *J. Mol. Biol. 117*, 607−620.
31. Lin, S. W., and Mathies, R. A. (1989) *Biophys. J. 56*, 653−660.
32. Huang, J. Y., and Lewis, A. (1989) *Biophys. J. 55*, 835−842.
33. Earnest, T. N., Roepe, P., Braiman, M. S., Gillespie, J., and Rothschild, K. J. (1986) *Biochemistry 25*, 7793−7798.
34. Park, M. H., Yamamoto, T., and Nakanishi, K. (1989) *J. Am. Chem. Soc. 111*, 4997−4998.
35. Zhang, H., Lerro, K. A., Takekuma, S., Baek, D., Moquin-Pattey, C., Boehm, M. F., and Nakanishi, K. (1994) *J. Am. Chem. Soc. 116*, 6823−6831.
36. Shi, G.-q., Cao, Z.-y., and Zhang, X.-b. (1995) *J. Org. Chem. 60*, 6608−6611.
37. Aksela, R., and Oehlschlager, A. C. (1991) *Tetrahedron 47*, 1163−1176.
38. Corey, E. J., Gilman, N. W., and Ganem, B. E. (1968) *J. Am. Chem. Soc. 90*, 5616−5617.
39. Oesterhelt, D., and Stoeckenius, W. (1974) *Methods Enzymol. 31*, 667−678.
40. Griffin, R. G. (1981) *Methods Enzymol. 72*, 108−174.
41. Ulrich, A. S., and Watts, A. (1993) *Solid State Nucl. Magn. Reson. 2*, 21−36.
42. Brown, M. F., and Chan, S. I. (1995) in *Encyclopedia of Nuclear Magnetic Resonance* (Grant, D. M., and Harris, R. K., Eds.) Vol. 2, pp 871−885, Wiley.
43. Henschel, R., Sillescu, H., and Spiess, H. W. (1980) *Polymer 22*, 1516−1521.
44. Schmidt-Rohr, K., Hehn, M., Schaefer, D., and Spiess, H. W. (1992) *J. Chem. Phys. 97*, 2247−2262.
45. Bloom, M., Davis, J. H., and Valic, M. I. (1980) *Can. J. Phys. 58*, 1510−1517.
46. Nevzorov, A. A., Moltke, S., and Brown, M. F. (1998) *J. Am. Chem. Soc. 120*, 4798−4805.
47. Fahmy, K., Siebert, F., Grossjean, M. F., and Tavan, P. (1989) *J. Mol. Struct. 214*, 257−288.
48. Fahmy, K., Siebert, F., and Tavan, P. (1991) *Biophys. J. 60*, 989−1001.
49. Drikos, G., and Rüppel, H. (1984) *Photochem. Photobiol. 40*, 93−104.
50. Schertler, G. F. X., Lozier, R., Michel, H., and Oesterhelt, D. (1991) *EMBO J. 10*, 2353−2361.
51. Stam, C. H. (1972) *Acta Crystallogr. 28B*, 2936−2945.
52. Hamanaka, T., and Mitsui, T. (1972) *Acta Crystallogr. 28B*, 214−222.
53. Tjandra, N., and Bax, A. (1997) *Science 278*, 1111−1114.

BI980676V